INSTABILITIES SIMULATIONS WITH WIDEBAND FEEDBACK SYSTEMS: CMAD, HEADTAIL, WARP

Kevin Li *, J. Cesaratto, J.D. Fox, M. Pivi, C. Rivetta,
SLAC, 2575 Sand Hill Road, Menlo Park CA, USA
G. Rumolo,
CERN, Geneva, Switzerland

Abstract

Transverse mode coupling (TMCI) and electron cloud instabilities (ECI) pose fundamental limitations on the acceptable beam intensities in the SPS at CERN. This in turn limits the ultimate achievable luminosity in the LHC. Therefore, future luminosity upgrades foresee methods for evading TMCI as well as ECI. Proposed approaches within the LHC Injector Upgrade (LIU) project include new optics with reduced transition energy as well as vacuum chamber coating techniques. As a complementary option, high bandwidth feedback systems may provide instability mitigation by actively damping the intra-bunch motion of unstable modes. In an effort to evaluate the potentials and limitations of such feedback systems and to characterise some of the specifications, a numerical model of a realistic feedback system has been developed and integrated into available instabilities simulation codes. Together with the implementation of this new feedback system model, CMAD and HEADTAIL have been used to investigate the impact of different wideband feedback systems on ECI in the SPS. In this paper, we present some details on the numerical model of the realistic feedback system and its implementation as well as the results obtained from the simulation study using this model together with the instability codes.

INTRODUCTION

Transverse mode coupling (TMCI) and electron cloud instabilities (ECI) pose fundamental limitations on the acceptable beam intensities in the SPS at CERN [1, 2]. With the ultimate goal to reliably provide the LHC with the beam required for High Luminosity LHC, different schemes are under investigation on how to evade both TMCI and ECI. Proposed approaches include lowering the transition energy in the SPS and thus increasing the synchrotron tune which has shown to increase the instability threshold for TMCI as well as stabilising the beam against ECI [2, 3]. Another approach is to coat the inside of the SPS vacuum pipes with low secondary electron yield (SEY) materials in order to diminish the natural SEY of the vacuum pipe and thus effectively suppressing the electron cloud build-up, thus stabilising the beam against ECI [4].

As a complementary option, high bandwidth feedback systems are under investigation to provide instability mitigation by actively damping selected intra-bunch modes that tend to become unstable by means of either TMCI or ECI [5]. With typical rms bunch lengths in the SPS in the order of 1 ns and unstable modes reaching up to mode 3 or higher, bandwidths of up to 1 GHz are required in order for the feedback system to resolve the intra-bunch motion. At high power levels, the design of such systems becomes technically very challenging.

In an effort to study and to characterise the potential effectiveness of such systems for damping TMCI or ECI, a numerical model of a realistic feedback system has been developed that does not only include bandwidth limitation but also models saturation as well as noise in the receiver and the kicker channels. This feedback model has been implemented in the instability codes CMAD [6], HEADTAIL [7] and WARP [8] allowing to study the impact of the feedback system on the beam within a machine environment. This is also a continuation of previous work conducted by Thompson [10] or by Ohmi [11].

The study presented, focuses on mitigation of ECI using the feedback system model with HEADTAIL-ElectronCloud flavour. The study of TMCI will be possible using the feedback system model with HEADTAIL-Impedance flavour due to its ability to communicate with the SPS impedance database. For this, the feedback system model has been implemented in an object-oriented manner to provide full modularity and ease the implementation in either of the flavours.

This paper presents an initial study which uses the HEADTAIL beam dynamics and feedback model to estimate the system impact of finite bandwidth kicker elements. We study closed-loop dynamics for kicker bandwidths of 200 MHz to 1 GHz. In these studies the feedback models are ideal (no additive noise in any processing components, no receiver sensitivity to charge in the bunch distribution, no saturation or power limits in the drive amplifier systems, etc.). These initial studies must be followed with more detailed studies to ultimately characterize the necessary system specifications for a potential feedback system in order to evaluate the cost vs. benefit and to line up the wideband feedback systems with the low transition energy optics and the low secondary electron yield coatings.

* Also at CERN, Geneva, Switzerland

NUMERICAL MODEL

In the following section we give a brief overview over the numerical modelling of the beam dynamics and the feedback system. Furthermore, we quickly elaborate on the implementation strategy for integration of the realistic feedback system in HEADTAIL.

Particle tracking

Particle tracking is realised as a second order symplectic advancement of phase space by combination of optics propagators and collective interactions which naturally inherently calls for multi-particle tracking.

The Hamiltonian for the full system is split into one part containing the (linear) machine optics and one part containing the collective effects. The Hamiltonian for the machine optics reads

$$H_{\text{optics}} = \frac{1}{2}\,p^2 + \frac{1}{2}\,K(s)^2\,x^2\,, \tag{1}$$

the independent variable is the path length s along the ring. It is second order in the canonical variables, hence, it generates a linear symplectic transformation of these variables, which can be expressed as the symplectic transfer matrix

$$M(x|x_0) = \exp\left(:-H\,s:\right) = I\,\cos(\mu) + S\,A\,\sin(\mu)\,, \tag{2}$$

where μ is the phase advance, S is the symplectic structure matrix, and A is a symmetric matrix parametrised by the Courant-Snyder parameters

$$A = \begin{pmatrix} \gamma & \alpha \\ \alpha & \beta \end{pmatrix}\,.$$

With $K(s)$ periodic, this leads to the solutions

$$\begin{aligned} x &= \sqrt{2\,J\,\beta(s)}\cos(\mu(s))\,, \\ p &= \sqrt{\frac{2\,J}{\beta(s)}}\left(\frac{\beta'(s)}{2}\,\cos(\mu(s)) - \sin(\mu(s))\right)\,, \end{aligned}$$

where J is the action and $\beta(s)$ is the betatron function.

The Hamiltonian for the collective effects is given as

$$\begin{aligned} H_{\text{coll.}} = \frac{p_e^2}{2m} &- \int d^3x\,\rho_p V_e - \frac{1}{4}\int d^3x\,F_{\mu\nu;\,e}F_{\mu\nu;\,e} \\ &+ T_p^2 - \int d^3x\,\rho_e V_p - \frac{1}{4}\int d^3x\,F_{\mu\nu;\,p}F_{\mu\nu;\,p} \\ &- \frac{r_0}{T_0\gamma c}\,y\sum_{k=1}^{N-\text{taps}} D_p(z-kC)\,K(z)\,, \end{aligned} \tag{3}$$

the independent variable is the time t. $F_{\mu\nu}$ are the electromagnetic field tensors [1]. In eq. (3), the first line includes the dynamics of the electron cloud particles and fields and the second line includes the dynamics of the beam particles and fields. The first and the last terms in each line contain the dynamics of the free particles and fields, the central terms provide the coupling between the charged particles and fields, respectively. As seen in eq. (3), the self-fields of the beam and the cloud are neglected. Neglecting the beam self-fields is valid under the assumption highly relativistic beams whereas neglecting the cloud self-fields is valid under the assumption of low electron cloud densities compared to the bunch density. Finally, the last line in eq. (3) describes the impact of the feedback kicker depending on the signal of the previous N-tap turns, $D_p(z-kC)$ is the corresponding dipolar moment of a beam slice and $K(z)$ is the kicker transfer function.

The one turn map along the full ring with N interaction points, representing the second order symplectic advancement of phase space and implemented numerically as a leap-frog scheme, can then be expressed as

$$M_{0\to N} = \sum_{i=0}^{N-1} e^{:-J\,\frac{\Delta\mu}{2}:}\,e^{:-H_{\text{coll}}\,\Delta t:}\,e^{:J\,\frac{\Delta\mu}{2}:}\,. \tag{4}$$

Numerically, the machine optics is established by means of the Courant-Snyder parameters either in smooth approximation or from a MAD-X lattice. The bunch is tracked from one point along the ring to the next via the transfer matrix M as

$$M = \begin{pmatrix} \sqrt{\beta} & 0 \\ -\frac{\alpha}{\sqrt{\beta}} & \frac{1}{\sqrt{\beta}} \end{pmatrix} \tag{5}$$

$$\times \begin{pmatrix} \cos(\mu_0+\Delta\mu) & \sin(\mu_0+\Delta\mu) \\ -\sin(\mu_0+\Delta\mu) & \cos(\mu_0+\Delta\mu) \end{pmatrix} \tag{6}$$

$$\times \begin{pmatrix} \frac{1}{\sqrt{\beta}} & 0 \\ \frac{\alpha}{\sqrt{\beta}} & \sqrt{\beta} \end{pmatrix}\,. \tag{7}$$

Single particle tune shifts are implemented explicitly via chromaticity and detuning parameters as

$$\begin{aligned} \Delta\mu_x &= \xi_x'\delta + \alpha_{xx}J_x + \alpha_{xy}J_y\,, \\ \Delta\mu_y &= \xi_y'\delta + \alpha_{xy}J_x + \alpha_{yy}J_y\,. \end{aligned}$$

Collective interaction with an electron cloud is computed on a slice-by-slice basis using a 2D integrated Green's function FFT-type Poisson solver. Interaction with the feedback system is also computed on a slice-by-slice basis taking into account different filters for receiver and kicker as well as saturation and noise. The feedback system can be operated in open or closed loop. The latter includes a processing channel with intrinsic delay storing the signals of N previous turns in forward and reverse registers allowing effectively to represent an N-tap filter.

Numerically, the impact of all feedback system components is handled by transfer matrices as illustrated in Fig. 1. The receiver filter samples the n_{slices} bunch slices to n_{channels} pickup channels, which may accumulate noise from the receiver and are then passed through the processing channel, which sets the phases and thus influences the damping rate of the feedback loop. The output signal can

[1] Eq. (3) is clearly not manifest covariant, consistently illustrating how the Hamiltonian is not a Lorentz invariant quantity.

be scaled by some additional scale gain factor [2]. It may accumulate noise from the amplifier before the kicker filter samples the n_{channels} kicker channels to n_{slices} bunch slices and the correcting kicks are applied to all slices, thereafter.

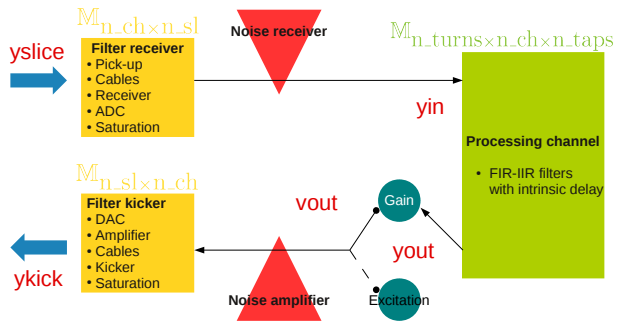

Figure 1: Schematic of the feedback system implementation along with indication of the transfer matrices and their dimensionalities.

Details on the modeling of the feedback system itself can be found in [9].

Implementation

The realistic feedback model was implemented into HEADTAIL in a modular manner as an independent C++ class allowing easy implementation in either of the two flavours (ElectronCloud and Impedance). The feedback system is fully initialised by means of the class constructor. The feedback system requires six input files each of which specify the transfer functions for the receiver and for the kicker, noise for the receiver and for the amplifier and the coefficients for the forward and the reverse controller of the FIR filter. The class constructor automatically detects the sampling rates and number of processing channels along with the number of turns for the noise and the number of delay-taps from the input files and resets any parameter that might have been misconfigured in the input file (raising a warning to the standard output). That way, the main function requires some slight adaption, essentially the addition of six lines to initialise the feedback system and adapt the number of slices and the number of turns, to register the beam signal at the pickup and to apply the correcting kicks for each slice.

The locations of the pickup and the kicker can be specified in the input file. In addition, the saturation levels can be set for the receiver and for the amplifier. The feedback system can be run using the actual slice offset from the simulation but also using the more realistic delta signal measured by the pickup. Furthermore, it can be run in closed or in open loop, the latter allowing to simulate an excitation of the beam by an external signal which can be injected via one of the noise files.

[2]The scale gain does not directly relate to the open-loop gain in any way.

SIMULATION RESULTS

In this study we focus on the evaluation of four kicker models, with bandwidths 200 MHz, 500 MHz, 700 MHz and 1 GHz - all described by perfect low-pass filter functions with first order phase response. All the other feedback components are assumed to be ideal (e.g. the pickup and receiver system have no noise floor or resolution limit, the receiver measurement of each bunch slice is assumed to be independent of the charge in that slice, the amplifier components have no power limit or saturation effects and the processing filter has no quantizing noise impact or numeric noise floor). Figure 2 shows the general frequency response of the 5 tap FIR filter in the processing channel. The five coefficients are plotted for each turn delay. Figure 2 also highlights the amplitude is at a maximum with the phase shifted by 90 degrees around the machine tune. The phase can be easily adjusted and depends on the separation of the pickup and the kicker along the ring. In our case, the separation was close to $0 \pmod{2\pi}$, hence, a 90 degree phase shift provides the optimum damping efficiency. The identical FIR filter was used for all the four feedback systems.

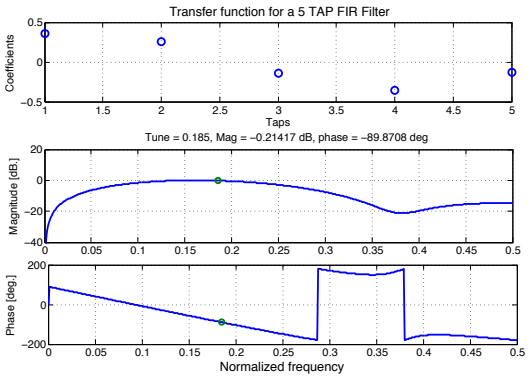

Figure 2: Magnitude and phase behaviour of the FIR filter vs. fractional tunes.

Figure 3 shows the kicker transfer functions of each of the feedback systems. Naturally, the roll-off of the frequency response takes place at lower frequencies for the low bandwidth systems. Apart from this feature, however, the frequency response shows the same characteristics for all systems.

The machine and beam parameters are collected in table. 1. They correspond to a nominal SPS beam at injection energy.

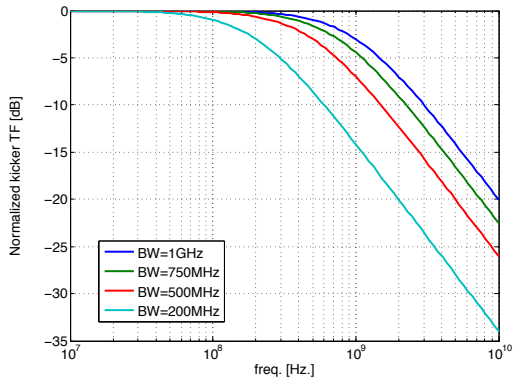

Figure 3: Kicker transfer functions for kicker bandwidths of 200 MHz, 500 MHz, 700 MHz and 1 GHz.

Intensity	1.1×10^{11} [ppb]
Energy	26 [GeV]
Emittances $[\varepsilon_x^n, \varepsilon_y^n]$	2.8, 2.8 [µm]
Beta functions $[\beta_x, \beta_y]$	42, 42 [m]
Tunes $[Q_x, Q_y, Q_s]$	26.13, 26.185, 0.0059
E-cloud regions	Bending magnets

Table 1: SPS machine settings at injection energy.

Damping the centroid motion

As an initial test, the impact of the feedback system on the centroid motion was investigated. For this, a single bunch was injected with an initial vertical offset of 2 mm. Four different feedback systems with bandwidths of 200 MHz, 500 MHz, 700 MHz and 1 GHz, respectively, were used to damp the injection oscillation using different scale gains. Figure 4 shows the results of the centroid motion for the 200 MHz and the 500 MHz feedback systems. The plot for the 200 MHz system exhibits the reduced gain acceptance as the eigenvalues shift out of the stability region for high gains. For the 500 MHz system all gains stabilise the centroid motion.

In Fig. 5 the damping times are plotted versus the scale gains for all feedback system. As expected all feedback systems perform equally well in damping the centroid motion since the bandwidths are sufficient in resolving the full bunch motion. What is different, though, is the gain acceptance, as already seen in Fig. 4. Higher bandwidths provide a higher gain acceptance and this can become a crucial property for cases where coherent beam instabilities are actually driven.

Electron cloud instabilities in the SPS

Having tested the feedback systems in the absence of electron clouds, next, the effect of electron clouds was investigated in the absence of a feedback system. This was done to acquire an idea of the beam behaviour under the impact of electron clouds in order to characterise the properties of the isolated ECI. This then finally allows to estimate the properties required for a feedback system in order to combat the driven ECI.

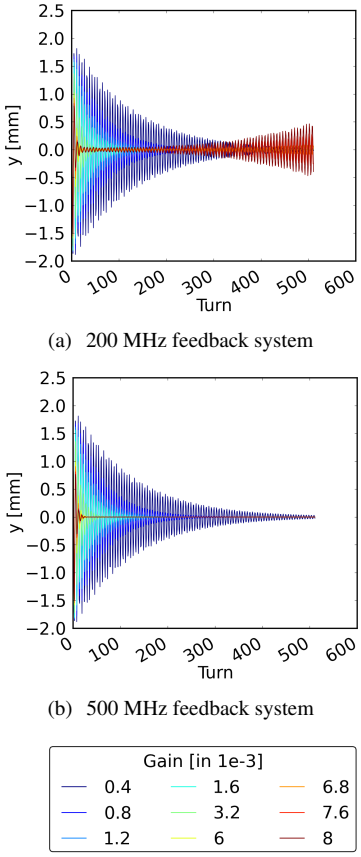

(a) 200 MHz feedback system

(b) 500 MHz feedback system

Figure 4: The evolution of the bunch centroid motion for different scale gains for the 200 MHz and the 500 MHz feedback systems.

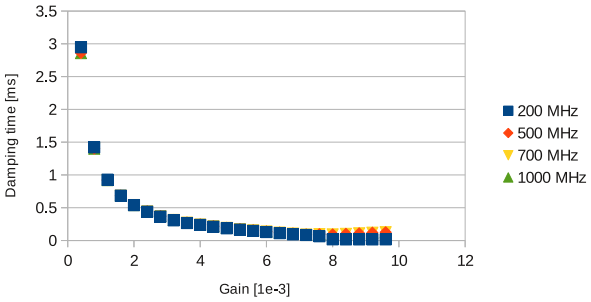

Figure 5: The damping times vs. scale gains for the four feedback systems for the damping of injection oscillations.

Fig. 6 shows the evolution of the centroid motion and the normalised emittance in the vertical plane for different central cloud densities. The instability threshold appears to be around 4×10^{11} m^{-3}. Above this cloud density, the coherent motion and the emittance grow rapidly up to densities of above 1×10^{12} m^{-3} where the emittance seems to saturate and to actually decrease as the density is fur-

ther increased. This may be attributed to Landau damping that can become effective as a result of the strong nonlinear fields generated by these very intense electron clouds.

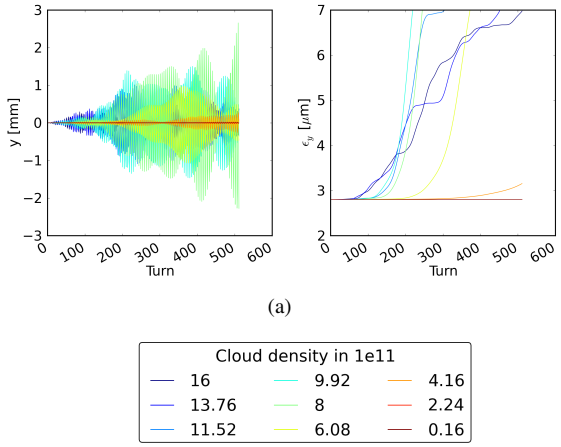

Figure 6: The evolution of the bunch centroid motion and the normalised emittance for different central cloud densities.

Figure 7 shows the mode picture for a region of central cloud density ranging from 0 to 1.6×10^{12} m^{-3}. The power spectrum is normalised for each density. Dark spots refer to maximum power, light spots indicate there is only little power contained in the respective mode. It is clearly visible that mode 0 dominates the coherent motion below the instability threshold. As the beam becomes unstable, mode -1 and for higher intensities even mode 2 become dominant. For very high densities the power returns back to mode 0.

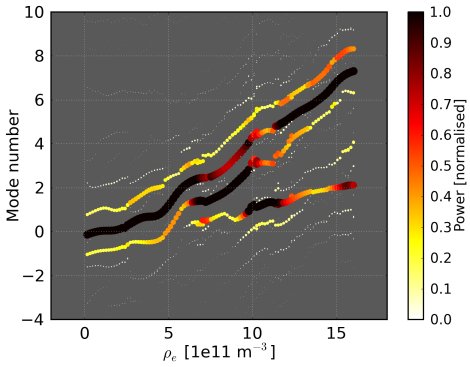

Figure 7: The mode spectrum for different central cloud densities. The spectrum is normalised for each density. Dark spots indicate modes containing high power, lighter spots are modes with less power.

Figure 8 shows a time domain picture of the bunch over several turns displaying a hybrid mode 0-1. This can also be seen in the mode picture in Fig. 9 where the dominant mode is a mode 0 shifted by approximately two synchrotron sidebands [3].

[3] See Fig. 7 for comparison.

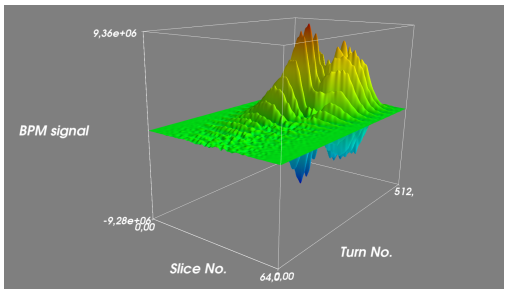

Figure 8: A time domain picture of an ECI for a central cloud density of $\rho_e \approx 6 \times 10^{11}$ m^{-3}.

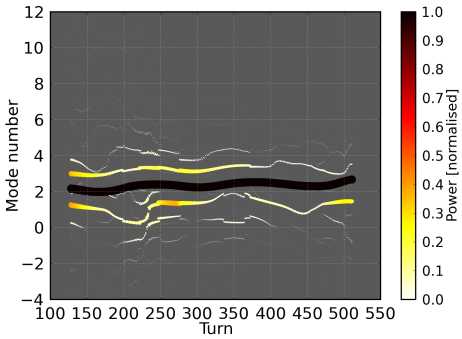

Figure 9: A frequency domain picture of an ECI for a central cloud density of $\rho_e \approx 6 \times 10^{11}$ m^{-3}. The power is concentrated mainly in modes 0 and 1.

The implications of this is that, under the presented conditions, a potential feedback system needs to be able to resolve mode 1 or perhaps mode 2 which suggests a bandwidth between 500 MHz to 750 MHz to be sufficient in order to stabilise a beam driven by an ECI. The following section will deal with this hypothesis by combining the impacts of electron clouds and feedback systems.

Damping the intra-bunch motion

Finally, the most interesting part is testing the performance of the different feedback systems on the beam in an electron cloud environment. For this the beam was tracked through the SPS with a central cloud density fixed at 6×10^{11} m^{-3} well above the instability threshold. With the beam under the constant impact of the electron clouds, the feedback systems were used to maintain stability.

Figure 10 shows that the beam can not be stabilised using a 200 MHz feedback system. Increasing the gain does reduce the instability rise time. However, before the instability can be fully damped, the gain acceptance of the system is exceeded and the feedback system itself drives the beam unstable again. This has already been observed in section where the 200 MHz system was used to damp the injection oscillations of the centroid motion. For that case, low gains were sufficient to damp the centroid motion, however.

Instead, the 500 MHz system has a higher gain accep-

tance and the gains can be increased so that the beam can actually be stabilised as shown in Fig. 10. From there, a scale gain factor of 6×10^{-3} is required to fully mitigate an ECI.

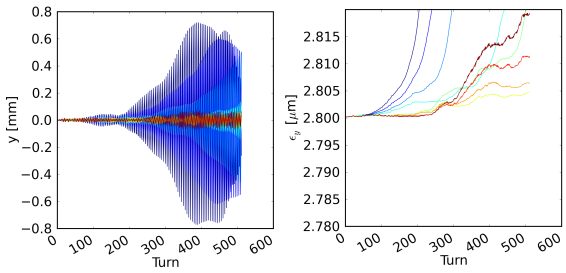

(a) 200 MHz feedback system

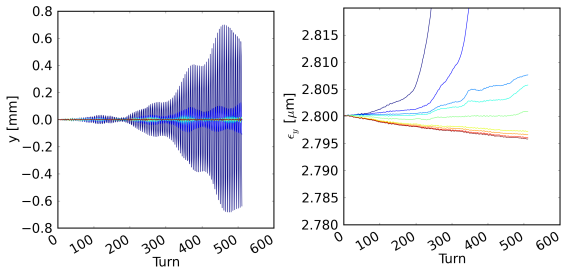

(b) 500 MHz feedback system

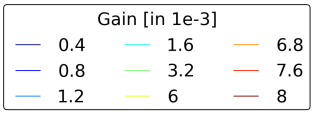

Figure 10: The evolution of the bunch centroid motion and the normalised emittance for different scale gains for the 200 MHz and the 500 MHz feedback systems.

Performing a central density scan using the 500 MHz feedback system at this scale gain level, shows the remaining power is distributed over a wide range of the mode spectrum concentrated more in the higher order modes as indicated by Fig. 11.

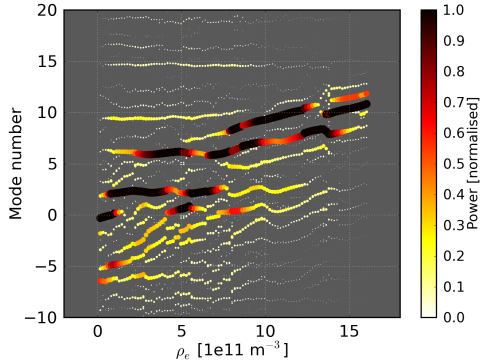

Figure 11: The mode spectrum for different central cloud densities. The spectrum is normalised for each density. Dark spots indicate modes containing high power, lighter spots are modes with less power.

Figure 12 shows the time domain picture of the bunch over several turns with the 500 MHz system at a scale gain of 6×10^{-3} and a constant cloud density of 6×10^{11} m^{-3}. The mode picture in Fig. 13 reveals a distribution of the remaining power mainly over modes 2 and 6.

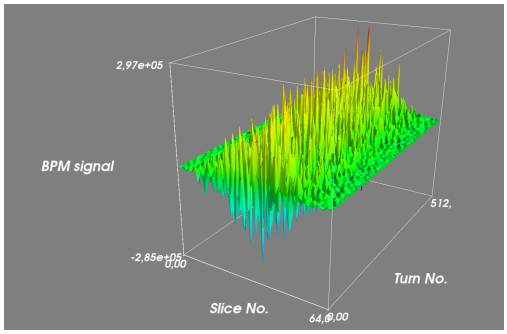

Figure 12: A time domain picture of an ECI damped with a 500 MHz feedback system at a scale gain of 6×10^{-3} for a central cloud density of $\rho_e \approx 6 \times 10^{11}$ m^{-3}.

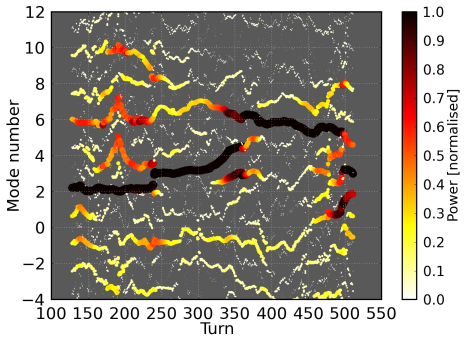

Figure 13: A frequency domain picture of an ECI damped with a 500 MHz feedback system at a scale gain of 6×10^{-3} for a central cloud density of $\rho_e \approx 6 \times 10^{11}$ m^{-3}. The remaining power is distributed mainly over modes 2 and 6.

Figure 13 also indicates that as the cloud density reaches very high levels, more power is accumulated in mode 6. An instability at these levels of cloud density should, therefore, no longer be accessible by the 500 MHz feedback system. Figure 14 shows a time domain picture of the bunch over several turns with the 500 MHz system at a scale gain of 6×10^{-3} and a constant cloud density of 1.4×10^{12} m^{-3}. The beam is unstable at this point. Both the time domain picture and the mode picture in Fig. 15, where the dominant mode is a mode 6 shifted by approximately four synchrotron sidebands [4], show a clear signature of a mode 6 instability.

[4] See Fig. 11 for comparison.

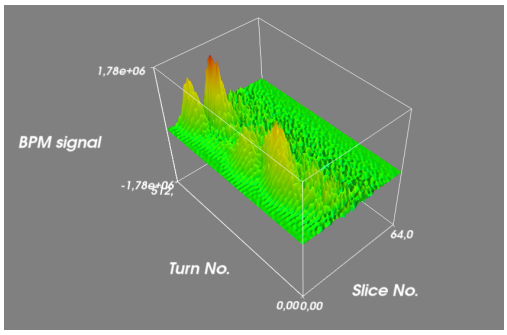

Figure 14: A time domain picture of an ECI for a central cloud density of $\rho_e \approx 1.4 \times 10^{12}$ m^{-3}.

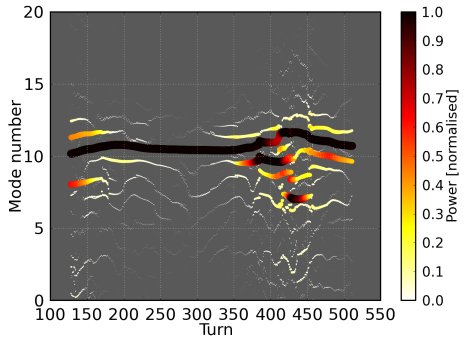

Figure 15: A frequency domain picture of an ECI for a central cloud density of $\rho_e \approx 1.4 \times 10^{12}$ m^{-3}. The power is concentrated in mode 6 (shifted to mode line 10).

CONCLUSIONS AND OUTLOOK

In the framework of the LIU project, a high bandwidth feedback system is under investigation for mitigation of TMCI and ECI. In this paper we have described the theoretical model of a realistic feedback system along with its implementation into the collective effects simulation code HEADTAIL. Using this combination of tools, different scenarios were explored to study the impact of potential feedback systems at bandwidths 200 mHz, 500 MHz, 700 MHz, and 1 GHz on the beam dynamics.

The studies showed that the centroid motion from injection oscillations could be effectively damped for all feedback systems. The damping rates depend on the overall gain of the system where the low bandwidth systems show less gain acceptance compared to higher bandwidth systems.

A reference case was then run for a nominal SPS beam at injection energy under the exclusive influence of electron clouds in order to characterise the isolated ECI. It could be shown that under these particular conditions the modes excited by an ECI are predominantly modes 0 and 1. Hence, for this beam, a feedback system with a minimum bandwidth of 500 MHz would be needed to suppress this type of instability.

Finally combining both the impact of the feedback system and the electron clouds in the particle tracking it was shown that while a 200 MHz system is insufficient to stabilise the beam against ECI, a 500 MHz system effectively provided mitigation of ECI up to cloud densities well above 1×10^{12} m^{-3}. At very high cloud densities above 1.4×10^{12} m^{-3} higher order modes arise from the ECI (mode 6 in our case) which can no longer be resolved by the 500 MHz system. The simulations indicate that should these density levels be reached, the bandwidths required may reach above 1 GHz.

In this study, the impact of kicker system bandwidth has been explored, but much work remains to quantify the impact of realistic feedback system limitations. The significance of a receiver noise floor, and a pickup-receiver system that measures a charge $\times$ displacement product, so that the effective gain of the feedback channel is reduced at the head and tail of the bunch, must be studied to understand how the residual motion of the controlled electron cloud system impacts the closed loop stability and modal content of the damped system. Another critical parameter to estimate is the behavior of the system with realistic injection transients, and nominal synchrotron motion from energy errors at injection, as these transients may be significant with regard to saturation effects in the processing and in the power stages (a study is necessary to estimate the impact of finite power levels and saturation effects). The behavior of the system during the energy ramp, and extraction, has not been quantified.

Finally, as realistic engineering specifications for possible pickups and kickers are developed, these parameters must be included into the feedback model of this simulation, so that the impact of realistic frequency and phase responses of potential engineering system elements can be better understood. There is much work to do, and opportunities to compare physical measurements of the real physical system, and this simulation, are also very significant in validating the results of these initial studies.

ACKNOWLEDGEMENTS

The authors would like to thank Alex Chao for valuable input and discussions.

REFERENCES

[1] B. Salvant, “Impedance model of the CERN SPS and aspects of LHC single-bunch stability.” PhD. thesis, Thse EPFL, no 4585 (2010).

[2] H. Bartosik et al., “Experimental Studies with Low Transition Energy Optics in the SPS”, Proceedings of IPAC 2011, San Sebastin, Spain, 2011.

[3] H. Bartosik et al., “Impact of Low Transition Energy Optics to the Electron Cloud Instability of LHC Beams in the SPS”, Proceedings of IPAC 2011, San Sebastin, Spain, 2011.

[4] C. Yin Vallrgen, “Low Secondary Electron Yield Carbon Coatings for Electron Cloud Mitigation in Modern Particle Accelerators” PhD. thesis, CERN-THESIS-2011-063 (2011).

[5] J.D. Fox et. al., “Feedback Control of Ecloud Instabilities”, CERN Electron Cloud Mitigation Workshop 2008.

[6] M. Pivi, “CMAD: A New Self-consistent Parallel Code to Simulate the ELectron CLoud Build-up and Instabilities”, SLAC-PUB-12970, 2007.

[7] G. Rumolo and F. Zimmermann, “Practical User Guide for HEADTAIL”, CERN-SL-Note-2002-036, 2002.

[8] J.-L. Vay et al., “Initial Self-Consistent 3D Electron-Cloud Simulations of the LHC Beam with the Code WARP+POSINST”, Proceedings of PAC 2005, Knoxville, TN, United States, 2005.

[9] C. Rivetta et al., “Mathematical Models of Feedback Systems for Control of Intra-bunch Instabilities driven by E-Clouds and TMCI”, Proceedings of PAC 2011, New York, NY, USA, 2012.

[10] J.R. Thompson et al., “Initial Results of Simulation of a Damping System for Electron Cloud-Driven Instabilities in the CERN SPS ”, Proceedings of PAC 2009, Vancouver, British Columbia, Canada, 2009.

[11] K. Ohmi, “Ecloud in SPS Feedback”, CERN E-cloud meeting, Geneva, Switzerland, 2011.